Iranian Journal of Electrical and Electronic Engineering

Journal Homepage: ijeee.iust.ac.ir

Research Paper

Performance Enhancement of Disk-Type Multi-Speed Wound-Rotor Resolver

F. Tootoonchian*(C.A.), and M. Amiri*

Abstract: Multi-Speed resolvers are desirable position sensors for high performance closed-loop control of inverter driven machines due to their high accuracy. However, developing a winding with high number of poles with limited number of slots is a main challenge in achieving multi-speed function. Therefore, in this paper different winding configuration are proposed to achieve 5-X performance of a disk type wound-rotor resolver. Then, the best winding is chosen for experimental verification. In addition to the accuracy of the sensor, the optimal winding selection index is defined considering copper usage, number of winding layers (overlapping or non-overlapping configurations), the number of turns for each coil of the winding (variable or constant turn configurations), and the amplitude of the fundamental harmonic. An objective function is defined involving all the mentioned indices with different weights determined based on the importance of each index. Finally, a prototype of the sensor with the best winding is built and tested. The experimental measurements verify the results of the simulations that are obtained using 3-D time setting finite element analysis.

Keywords: Disk type wound rotor resolver, Resolver, Multi-speed sensor, 3-D time stepping finite element analysis, Winding configurations.

1 Introduction

POSITION sensors are widely used in closed-loop control of inverter driven machines [1]. There are different position sensors that among them Hall Effect sensors, optical encoders and resolvers are more commercial. The lowest cost is devoted to the Hall Effect sensors in the price of the worst accuracy [2]. In many industrial applications the required accuracy is higher than that of Hall sensors. In high performance control loops, the main competitors are optical encoders and resolvers [3].

Among them resolvers are more reliable for harsh environments, where wide temperature variations, high vibration level, and high pollution are existed [4].

There are two kinds of resolvers: Wound Rotor (WR) and Variable Reluctance (VR) ones. The excitation winding of the first is located on the rotor and fed using a high frequency sinusoidal voltage. The resulted flux is coupled with two-phase signal windings that are located on the stator side. The signal windings are connected to a high input impedance Resolver to Digital Converter (RDC) [5]. Therefore, the WR resolver can be assumed the same as an open circuit, two-phase synchronous generator with AC excitation. The induced voltages in signal windings are amplitude modulated signals whose envelopes are proportional to the sine and cosine of the rotor position. Therefore, the position can be determined using the inverse tangent of the voltages' ratio. Decoupling the carrier and calculating the

Iranian Journal of Electrical and Electronic Engineering, 2023.
Paper first received 20 Aug 2022, revised 23 Oct 2022, and accepted 08 Nov 2022.
*The authors are with the Department of Electrical and Electronic Engineering, Iran University of Science and Technology, Tehran, Iran.
E-mails: tootoonchian@iust.ac.ir and mohammad.amiri76@gmail.com.
Corresponding Author: F. Tootoonchian.
https://doi.org/10.22068/IJEEE.19.1.2628.

position is done using the RDC. Despite WR resolvers, in VR resolver the excitation winding is transferred to the stator side. It means all the signal and excitation windings are wound around the stator teeth [6]. The rotor is a winding less ferromagnetic core with a special shape to guarantee the sinusoidal variation of mutual inductance between the signals and the excitation windings. The commercial VR resolvers works based on the variation of air-gap length [7]. Therefore, their accuracy is strongly influenced by mechanical faults [8]. Although WR resolvers have less performance deterioration under mechanical faults with respect to VR ones, their accuracy is decreased under eccentricities. Disk-type resolvers are proposed to overcome this defect [9].

The literature on disk type resolvers can be divided into three groups:

1.1 Analytical Models for Disk Type Resolvers

Since disk type resolvers need 3-D time stepping finite element analysis for their performance evaluation and such analysis is very time consuming, there are lots of researches on proposing analytical models for their performance evaluation. Winding function model for disk type WR and sinusoidal area VR resolvers are proposed in [10] and [11], respectively. 3-D Magnetic Equivalent Circuit (MEC) model for WR resolvers is proposed in [12] and a hybrid model based on MEC and Conformal mapping method is proposed in [13] for disk type variable air-gap length VR resolver.

1.2 Performance Evaluation or Enhancement under Fault Condition

The performance of disk type sinusoidal area VR resolver under mechanical and electrical faults is discussed in [14]. The similar evaluations are done on sinusoidal air-gap length VR and WR resolvers in [15] and [13], respectively.

1.3 Accuracy improvement

Accuracy improvement for disk type resolvers is done based on different optimization variables. In [11] and [13] injecting harmonics to the rotor contour and using multi-speed configuration are discussed. In [16] disk type VR sensor is adjusted for limited angle position estimation. Winding proposal for multi-speed WR resolvers is considered in [17] based on Fractional Slot (FS) winding method. However, FS winding suffers from high level of sub-harmonics. To suppress those subharmonics, a new configuration, multi-stage slots, based on using multi-layer FS winding with specific shifting between layers is proposed for disk-type resolvers in [18]. However, in the proposed multi-stage resolver the shifting angle between different layers of the winding was limited by the slot opening width of the slot's lower layer. Therefore, to overcome that dilemma a slot-less disk type resolver is proposed in [19]. However, the objective function of presenting all the mentioned windings is achieving the minimum position error with no attention to winding facility, and phase separation.

In this paper, the accuracy improvement of disk type WR resolver is discussed based on defining optimal winding. Three different windings are proposed for the studied multi-speed resolver and the best winding considering higher accuracy, higher practical facility of winding, lower copper usage, and higher reliability/phase separation is determined. Finally, the optimal resolver is built and experimentally tested. Close agreement between the test and simulation results approved the presented results.

2 Structure of the Studied WR Resolver

The studied sensor is a disk type WR resolver. It has a single stator, single rotor configuration, as shown in Fig. 1. Both the stator and the rotor has 10-pole windings, therefore the sensor is a multi-speed (5-X) resolver. The stator has 28 slots and the rotor has 20 slots. Considering allowable slot-pole combinations the distributed winding is not possible for this resolver. Therefore, on-tooth winding is applied for both the stator and the rotor windings. The number of turns for the k^{th} tooth of the excitation winding is determined as:

$$N_{ek} = N_e \cos\left[(k-1)\frac{2p_w\pi}{Z_r}\right] \quad (1)$$

where N_e is the maximum number of excitation coils, p_w is number of pole pairs, and Z_r is number of rotor teeth.

The number of turns for the signal windings considering over-lapping variable turn configuration for the k^{th} tooth of the stator can be determined as:

$$N_{sk} = N_s \sin\left[(k-1)\frac{2p_w\pi}{Z_s}\right] \quad (2)$$

$$N_{ck} = N_s \cos\left[(k-1)\frac{2p_w\pi}{Z_s}\right] \quad (3)$$

where N_s and Z_s denote the maximum number of the signal coils and number of stator teeth, respectively.

Geometrical dimensions of the studied resolver are given in Table 1.

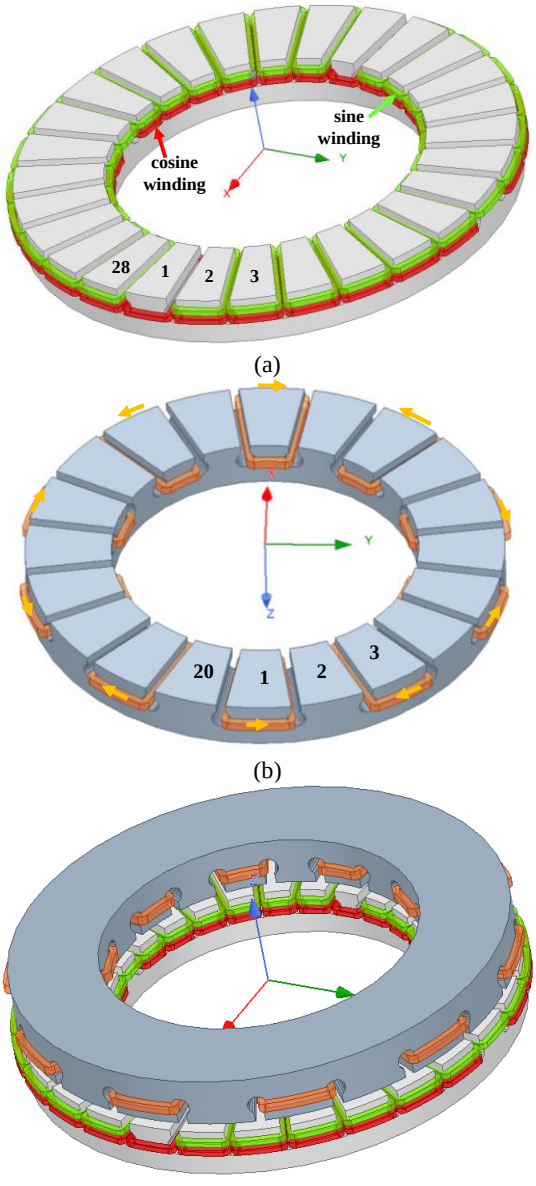

Fig. 1 The studied resolver, (a) the stator core, (b) the rotor core, and (c) the assembled resolver.

Table 1 Geometrical Dimension of the studied sensor.

Parameter	Unit	Value
Pole pairs	-	5
Air gap length	mm	0.5
Core outer/inner diameter	mm	50/32
Stator/rotor axial length	mm	5
Number of stator/rotor slots, Z_s/Z_r	-	28/20
Stator/rotor slots' radius	mm	1
Stator/rotor slots' slot opening width	mm	1
Stator/rotor slots' slot opening height	mm	1
Maximum number of excitation coils, N_e	-	70
Maximum number of signal coils, N_s	-	35

3 Principle of Operation

As mentioned earlier, the resolver can be assumed as a two-phase synchronous generator with AC excitation. The armature, signal, windings must be wound in such a way that their mutual inductance with the excitation winding varies sinusoidal, when rotor rotates. In addition, they must have 90-degree phase separation with each other. It means the mutual inductance between the excitation winding and the signal windings (sine and cosine windings), in ideal condition, can be written as:

$$L_{se} = M\sin(\theta_r) \quad (4)$$

$$L_{ce} = M\cos(\theta_r) \quad (5)$$

where L_{se} / L_{ce} is the mutual inductance between the sine/cosine and the excitation windings, M is the maximum value of the stator and rotor mutual inductance, and θ_r is the rotor position.

Furthermore, it is required to keep constant the self-inductance of the excitation winding to avoid including disturbing harmonics in the output voltages. Therefore, by suppling the excitation winding with a high frequency sinusoidal voltage, the excitation current in the steady state would have a constant amplitude with the same frequency as the excitation voltage. Hence, the linkage flux of the signal windings can be determined as:

$$\lambda_{sin} = (M\sin\theta_r)(I_m sin\omega_e t) \quad (6)$$

$$\lambda_{cos} = (M\cos\theta_r)(I_m sin\omega_e t) \quad (7)$$

where I_m is the maximum value of the excitation current and ω_e is the angular frequency of the excitation voltage. Then, the induced voltages in the signal windings can be calculated as:

$$V_{sin} = \omega_e M I_m\left(\frac{\dot{\theta}_r}{\omega_e}\cos\theta_r sin\omega_e t + sin\theta_r cos\omega_e t\right) \quad (8)$$

$$V_{cos} = \omega_e M I_m\left(-\frac{\dot{\theta}_r}{\omega_e}\sin\theta_r sin\omega_e t + cos\theta_r cos\omega_e t\right) \quad (9)$$

where $\dot{\theta}_r$ denotes the rotational speed of the rotor. Since for resolvers $\dot{\theta}_r \ll \omega_e$, the speed voltages can be ignored:

$$V_{sin} = \omega_e M I_m sin\theta_r cos\omega_e t \quad (10)$$

$$V_{cos} = \omega_e M I_m cos\theta_r cos\omega_e t \quad (11)$$

Therfore, the induced voltages are ampitude modulated signals that their carrier is the excitation signal of the resolver. The envelope of (10)-(11) can be determined as:

$$E_{sin} = \omega_e M I_m sin\theta_r \quad (12)$$

$$E_{cos} = \omega_e M I_m cos\theta_r \quad (13)$$

And then, the rotor position is calculated as:

And then, the rotor position is calculated as:

$$\theta_r = arctan\frac{E_{sin}}{E_{cos}} \quad (14)$$

In practice the mutual inductances between the signal and the excitation windings are not equal to the ideal forms of (4) to (5). Also, calculating the envelope of the voltages and the rotor position in RDC are accompanied by different errors. Therefore, the calculated position differs from the real position. The difference between the real position and the calculated one, is defined as the position error.

4 Performance Evaluation of the Initial Design

The most accurate method for performance evaluation of disk type resolvers is time transient, 3-dimentional finite element analysis. It considers the real geometry of the senor with no simplification, the real material used for building the sensor. However, it is required to consider the appropriate time step and mesh quality to ensure the reliable results. In addition, simulation must be done in a whole mechanical period of the sensor and the voltage source must be chosen for the excitation type.

The schematic of the mesh on the cores' body is shown in Fig. 2-a. The total number of mesh elements is 200402. It is worth mentioning that the mesh of Fig. 2-a, is generated in Magnetostatic solver and then imported to the transient solver. Considering the excitation frequency of 4 kHz, the time step is set equal to 15.625 μs. Since the rotational speed of the rotor is 600 rpm, the stop time of the simulation is set equal to 120 ms to ensure of having signals for more than one mechanical period of the sensor. In addition, the distribution of the magnetic flux density in the middle of the air-gap length at 120 ms is given in Fig. 2-b. As it can be seen the maximum amplitude of the magnetic flux density is 8.59 mT that is less than saturation level of the employed ferromagnetic core.

The induced voltages and their envelope are given in Fig. 3-a. Peak detection method is used for calculating the envelopes. Then, the harmonic content of the envelopes is shown in Fig. 3-b. The amplitude of the fundamental harmonic is 1.97 V, total harmonic distortion (THD) of the envelops is 0.87%. Since overlapping variable turn winding configuration is used for the signal windings, those grate results were predictable. Position error of the sensor with respect to the real position is given in Fig. 3-c.

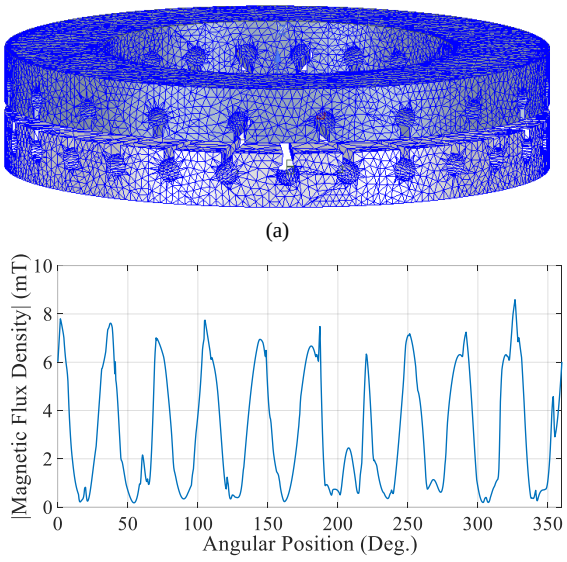

Fig. 2 (a) The schematic of the mesh on the cores' body, and (b) the distribution of the magnetic flux density in the middle of the air-gap length at t=120 ms.

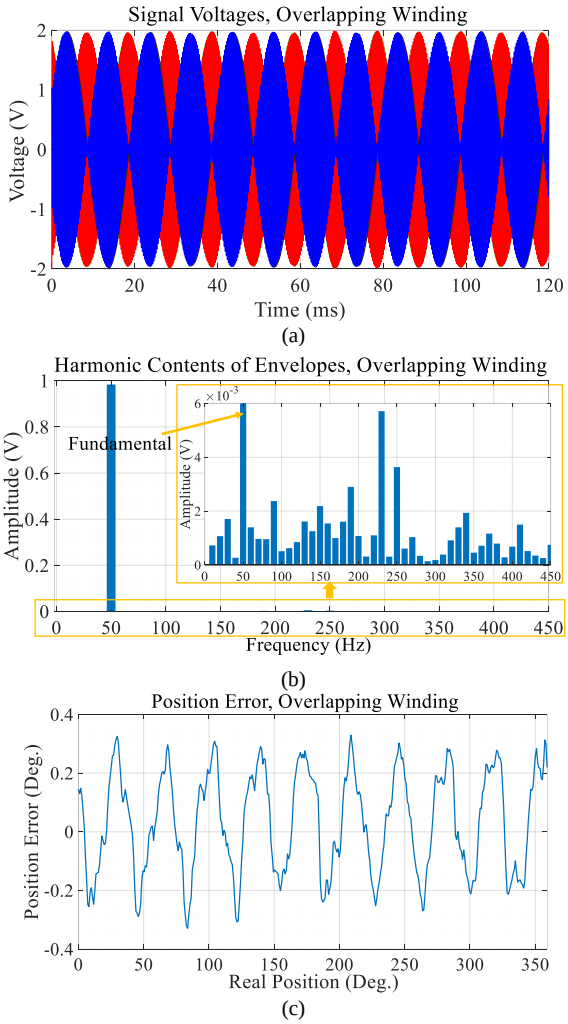

Fig. 3 The results of 3-D FEM for the studied resolver with variable turn, overlapping configuration for the signal windings: (a) the induced voltages and their envelope, (b) the harmonic content of voltages' envelope, and (c) the position error.

The Average of Absolut Position Error (AAPE), as the best index of resolver's accuracy is calculated equal to 0.239˚and the Peak to Peak Position Error (PPPE) is equal to 0.659˚. The value of position errors shows the initial design sensor is an accurate resolver. However, due to overlapping winding configuration, the probability of a short circuit fault is high. On the other hand, using variable turns for different coils of each winding, as well as high number of coils in the stator lead to hard practical implementation of the sensor and high copper consumption. Therefore, in the following, two other configurations are proposed for the stator windings to improve practical implementation of the studied resolver.

5 Performance Improvement

In order to improve the performance of the studied resolver, an objective function, , is defined as:

$$\xi = \frac{(AAPE)^{k_1} \times (NSC)^{k_2}}{(PFF)^{k_3} \times (AFH)^{k_4}} \quad (15)$$

where *NSC* is the Number of Stator Coils, *AFH* is the Amplitude of the Fundamental Harmonic, and *PFF* is Practical Facility Factor that can be defined as:

$$PFF = 1 + k_5 \times \alpha + k_6 \times \beta \quad (16)$$

where for non-overlapping winding, α=1 and overlapping one α=0. Also, for variable turn coils β=0 and for constant turn ones, β=1. The coefficients of k_1, k_2,…, k_6 are the constant values that are selected by designer's will. Giving the highest important to the accuracy of the sensor, k_1=2. The lower *NSC*s leads to lower copper usage. So, k_2 is selected equal to 1.2. Other coefficients are determined as: k_3=1.5, k_4=1, k_5=1, and k_6=2. Finally, it is worth mentioning that the value of *AAPE*, *NSC*, and *AFH* are normalized versus their best value for different windings to ensure the calculated objective function has no dimension.

Other possible configurations are non-overlapping winding that is presented in Fig. 4-a, and fractional slot winding of Fig. 4-b. As it can be seen in Fig. 4-a, the proposed winding has on-tooth, non-overlapping, variable turn configuration. The number of each coil's turn is determined based on (2)-(3). In fact, the number of turns for sine winding is determined using (2) for even teeth (k =2, 4, 6, …, 28). Also, the number of turns for cosine coils is calculated by (3) for odd teeth (k =1, 3, 5, …, 27).

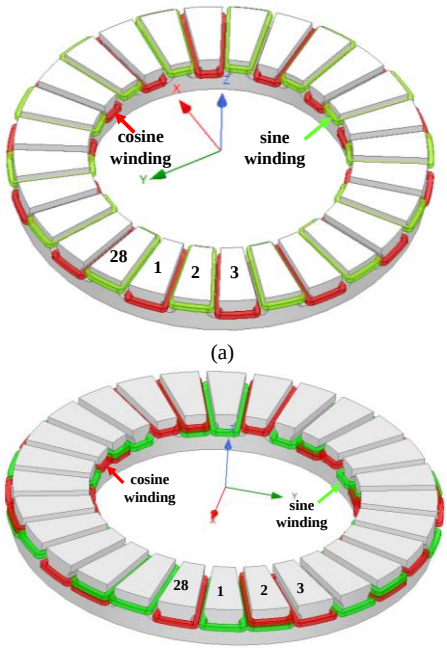

Fig. 4 The proposed windings for the stator: (a) the non-overlapping winding (b) The fractional slot winding.

The induced voltages in the signals windings, using the non-overlapping configuration, are shown in Fig. 5-a, along with the envelope of the voltages. The harmonic content of the envelopes are given in Fig. 5-b, and the position error of the sensor is shown in Fig. 5-c. As it can be seen from Fig. 5-b, the amplitude of the fundamental harmonic is 0.98 V which is less than that of the initial winding.

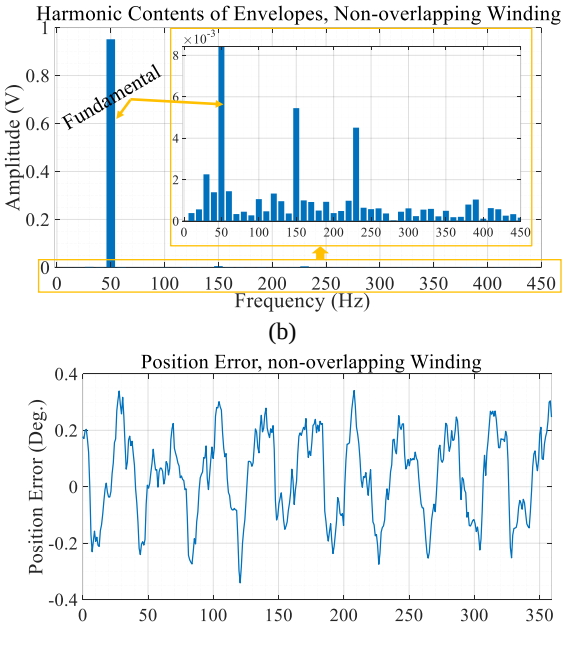

Fig. 5 The results of 3-D FEM for the studied resolver with variable turn, non-overlapping configuration for the signal windings: (a) the induced voltages and their envelope, (b) the harmonic content of voltages' envelope, and (c) the position error.

Of course, due to reducing the number of coils per each signal winding decreasing the amplitude of the fundamental harmonic was predictable. THD of envelopes, THD=1.12%, is also deteriorated with respect to the initial winding. AAPE and the PPPE for the non-overlapping winding are 0.199˚, and 0.682˚, respectively. These value shows that the number of coils decreases and the winding facility increases with respect to the initial design in the price of accuracy deterioration.

The induced voltages in the fractional slot windings and the envelopes' harmonic content are given in Figs. 6-a, and 6-b, respectively. THD of envelopes is 1.18% and the amplitude of the fundamental harmonic is 0.95 V. Both values are worse than those of overlapping winding. However, the position error, Fig. 6-c, shows AAPE and PPPE is equal to 0.075˚and 0.514˚, respectively.

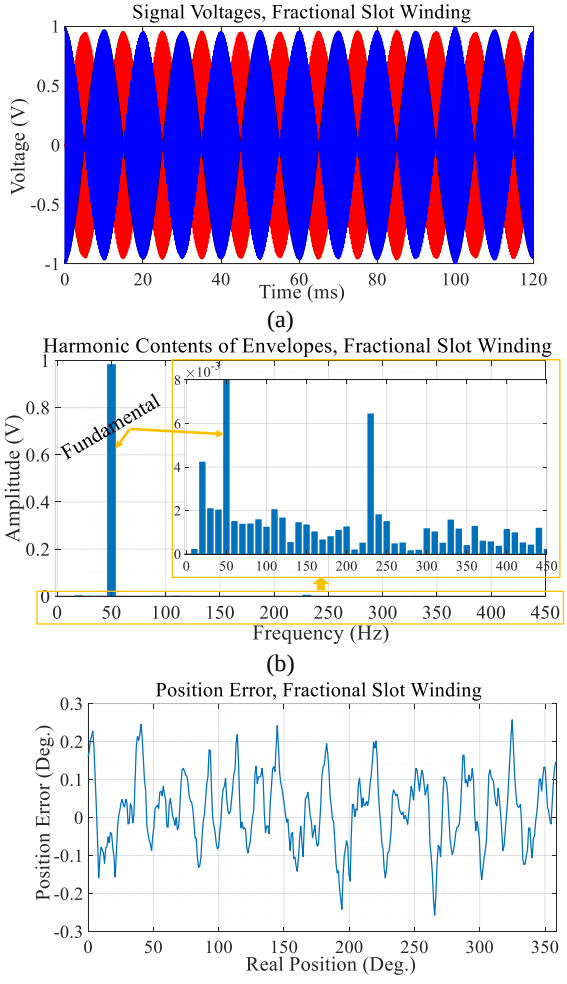

Fig. 6 The results of 3-D FEM for the studied resolver with fractional slot windings: (a) the induced voltages and their envelope, (b) the harmonic content of voltages' envelope, and (c) the position error.

It can be seen, using fractional slot winding leads to the most accurate resolver in comparison with two previous designs. It is worth mentioning that the number of turns for each coil is equal to 40. It means all coils have constant turns. Also, 8 teeth have been equipped with two-layer coils and the other teeth have non-overlapping coils.

The characteristics of different windings are summarized in Table 2. As given in Table 2, the best value of the proposed objective function is 0.540 that is referred to the fractional slot winding. Therefore, fractional slot winding is considered for practical verification.

6 Experimental Validation

The prototype of the resolver with fractional slot winding is built. The stator core is given in Fig. 7-a, and the rotor core is presented in Fig. 7-b.

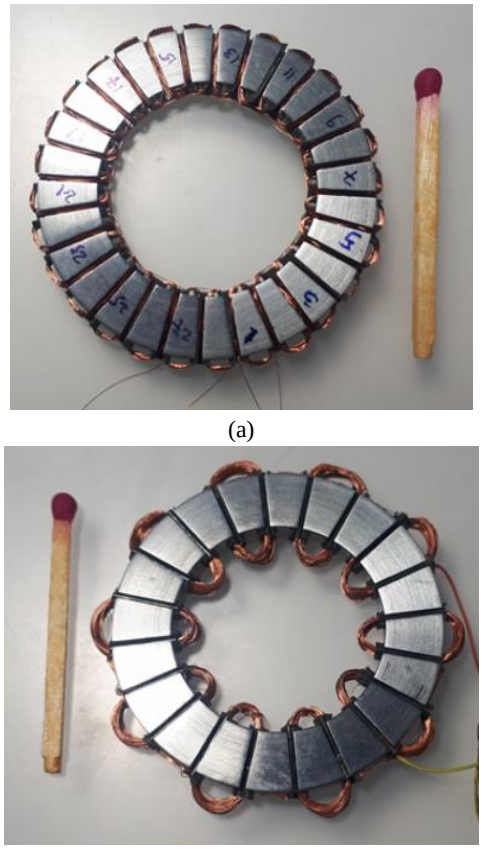

(a)

(b)

Fig. 7 The prototype resolver: (a) the stator, and (b) the rotor.

The built sensor is experimentally tested to verify its accuracy. The employed test circuit is given in Fig. 8. As it can be seen, a DC motor is used for rotating the rotor of the sensor. The excitation winding is fed using a function generator with a 4 kHz sinusoidal voltage.

Table 2 Comparing different windings, the best values are made **Bold**

Winding configuration	THD (%)	AAPE (Deg.)	PPPE (Deg.)	AFH (V)	NSC	α	β	ξ
Overlapping (initial design)	**0.871**	0.239	0.659	**1.97**	52	0	0	21.345
Non-overlapping	1.12	0.199	0.682	0.98	**28**	**1**	0	5.004
Fractional slot	1.18	**0.075**	**0.514**	0.95	36	0	**1**	0.540

The amplitude of this voltage can be adjusted using the automatic gain control circuit of the employed function generator. It is worth mention that feeding the rotating winding of the rotor is done brushless using a rotary transformer. The employed rotary transformer is shown in Fig. 8.

Its primary coil is fed using the function generator and the induced voltage in its secondary coil is used as the excitation voltage. Then, the induced voltages in the signal windings of the resolver, as shown in Fig. 9-a, are measured and captured using a digital oscilloscope. Those voltages are transferred to the Matlab software to decouple the carrier and calculate the envelopes. The position of the rotating shaft is calculated based on invers tangent of the envelope's ratio. In order to calculate the position error a reference position sensor is required. The employed position sensor is an optical encoder that is coupled to the DC motor.

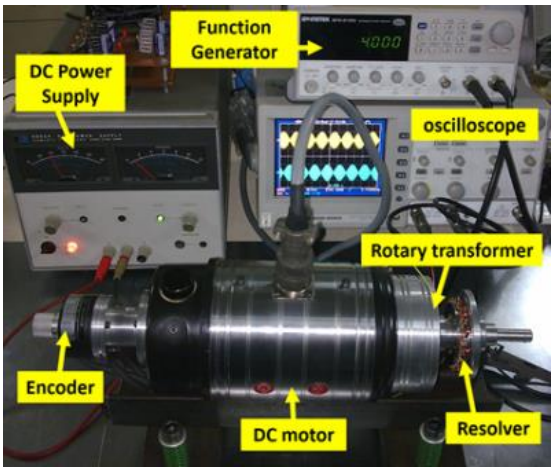

Fig. 8 The employed test circuit for experimental measurements.

Finally, the position error can be determined by comparing the estimated position by prototype resolver and that of reference sensor. Calculating the position error, shown in Fig. 9-b, shows the measured PPPE is 0.534 ˚ and the AAPE is 0.08 ˚. It means the deviation of the predicted values using finite element analysis with respect to the measured ones is less than 7%. Therefore, the experimental results verify the simulation ones.

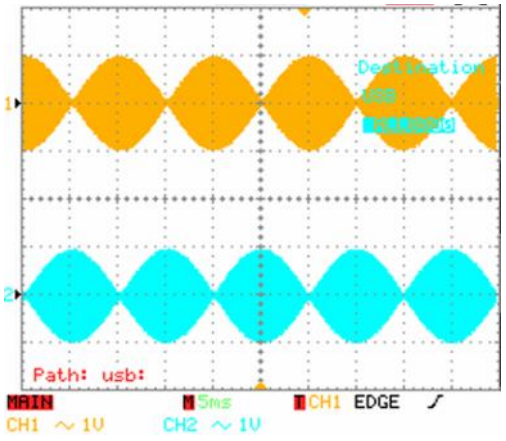

(a)

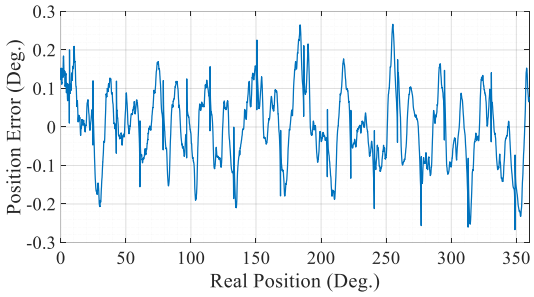

(b)

Fig. 9 The results of the experimental test: (a) the measured induced voltages, (b) position error.

To ensure the appropriate performance of the prototype, the experimental tests are repeated for different speeds. The analogue voltages for 100, 1000, and 1500 rpm are presented in Figs. 10-a, through 10-c. The PPPE and the AAPE for different speeds are given in Fig. 11 indicating no significant change.

7 Conclusion

In this paper, different winding configuration for multi-speed, disk type, wound rotor resolver was examined. An objective function considering accuracy of the sensor, number of stator coils (copper usage), amplitude of the fundamental harmonics, and facility of the winding process were proposed as preference index of the optimal winding. To determine the facility of winding, the winding type from overlapping or non-overlapping configuration point of view, as well as having variable- or constant-turn coils was considered.

Finally, fractional slot winding was chosen as the optimal winding with the lowest value of the objective function. The optimal resolver was practically built and tested. Close agreement between the results of 3-D time stepping finite element analysis and experimental measurements verify the performed analysis.

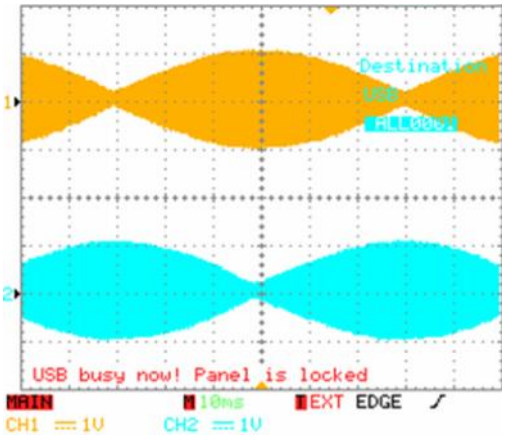

(a)

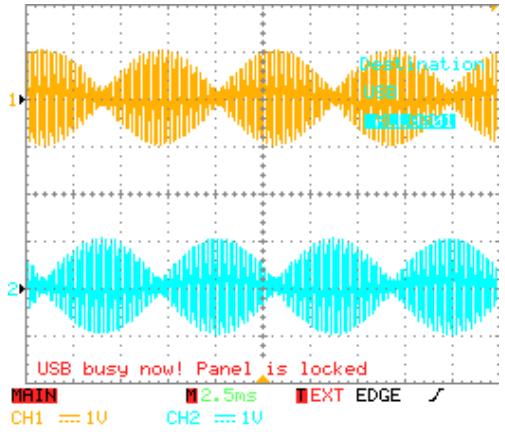

(b)

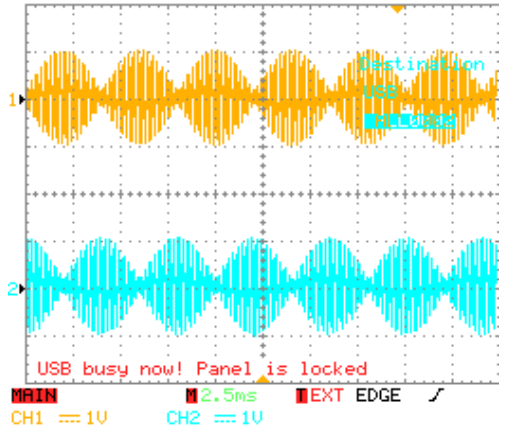

(c)

Fig. 10 The measured induced voltages for different speeds: (a) 100 rpm, (b) 1000 rpm, and (c) 1500 rpm.

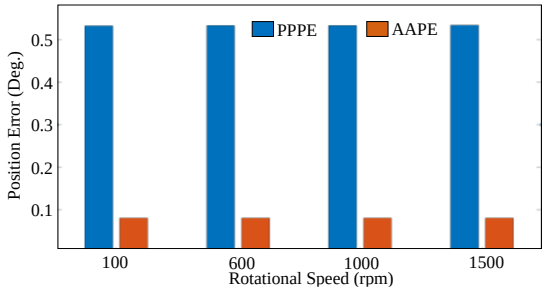

Fig. 11 The results of the experimental test for different speeds.

Intellectual Property

The authors confirm that they have given due consideration to the protection of intellectual property associated with this work and that there are no impediments to publication, including the timing to publication, with respect to intellectual property.

Funding

No funding was received for this work.

CRediT Authorship Contribution Statement

F. Tootoonchian: Idea & Conceptualization, Experimental measurements and prototyping, Supervision, Revise & Editing. **M. Amiri:** Software and Simulation.

Declaration of Competing Interest

The authors hereby confirm that the submitted manuscript is an original work and has not been published so far, is not under consideration for publication by any other journal and will not be submitted to any other journal until the decision will be made by this journal. All authors have approved the manuscript and agree with its submission to "Iranian Journal of Electrical and Electronic Engineering".

References

[1] P. Naderi and R. Ghandehari, "Comprehensive Analysis on a New Type VR-Resolver with Toroidal Windings Under Healthy and Eccentric Cases," in *IEEE Transactions on Industrial Electronics*, Vol. 69, No. 12, pp. 13754-13762, 2021.

[2] X. Ge, Z. Q. Zhu, R. Ren, J. T. Chen "A Novel variable reluctance resolver for HEV/EV applications", *IEEE Transactions on Industry Applications*, Vol. 52, No. 4, pp. 2872-2880, 2016.

[3] F. Zare and Z. Nasiri-Gheidari, "Helical Motion Wound-Rotor Resolver," *IEEE Sensors Journal*, Vol. 22, No. 10, pp. 9371-9377, 2022.

[4] T. Gundogdu, and B. Ozdincer, "Design and Analysis of Limited-Angle Wound Rotor Resolvers," *IEEE Sensors Journal*, Vol. 22, No. 10, pp. 9351-9360, 2022.

[5] F. Zare and Z. Nasiri-Gheidari, "Winding Function Model for Predicting Performance of 2-DOF Wound Rotor Resolver," *IEEE Transactions on Transportation Electrification*, Vol. 8, No. 2, pp. 2062-2069, 2022.

[6] H. Saneie and Z. Nasiri-Gheidari, "Generalized Nonoverlapping Tooth Coil Winding Method for Variable Reluctance Resolvers," *IEEE Transactions on Industrial Electronics*, Vol. 69, No. 5, pp. 5325-5332, 2021.

[7] R. Ghandehari, P. Naderi, and L. Vandevelde, "Performance Analysis of a New Type PM-Resolver in Healthy and Eccentric Cases by an Improved Parametric MEC Method," *IEEE Transactions on Instrumentation and Measurement*, Vol. 70, pp. 1-10, 2021.

[8] P. Naderi, R. Ghandehari, and M. Heidary, "A Comprehensive Analysis on the Healthy and Faulty Two Types VR-Resolvers with Eccentricity and Inter-Turn Faults," *IEEE Transactions on Energy Conversion*, Vol. 36, No. 4, pp. 3502-3511, 2021.

[9] Z. Nasiri-Gheidari, "Design, Analysis, and Prototyping of a New Wound-Rotor Axial Flux Brushless Resolver," *IEEE Transactions on Energy Conversion*, Vol. 32, No. 1, pp. 276-283, 2017.

[10] R. Alipour-Sarabi, Z. Nasiri-Gheidari, F. Tootoonchian, and H. Oraee, "Analysis of Winding Configurations and Slot-Pole Combinations in Fractional-Slots Resolvers", *IEEE Sensors Journal*, Vol. 17, No. 14, pp. 4420-4428, 2017.

[11] Z. Nasiri-Gheidari, R. Alipour-Sarabi, F. Tootoonchian, and F. Zare, "Performance Evaluation of Disk Type Variable Reluctance Resolvers," *IEEE Sensors Journal*, Vol. 17, No. 13, pp. 4037-4045, 2017.

[12] R. Alipour-Sarabi, Z. Nasiri-Gheidari, and H. Oraee, "Development of a Three-Dimensional Magnetic Equivalent Circuit Model for Axial Flux Machines," *IEEE Transactions on Industrial Electronics*, Vol. 67, No. 7, pp. 5758-5767, 2020.

[13] H. Saneie, Z. Nasiri-Gheidari, and F. Tootoonchian, "Design-Oriented Modelling of Axial-Flux Variable-Reluctance Resolver Based on Magnetic Equivalent Circuits and Schwarz–Christoffel Mapping," *IEEE Transactions on Industrial Electronics*, Vol. 65, No. 5, pp. 4322-4330, 2018.

[14] F. Tootoonchian, and F. Zare, "Performance analysis of disk type variable reluctance resolver under mechanical and electrical faults", *Iranian Journal of Electrical and Electronic Engineering*, Vol. 14, No. 3, pp. 299-307, 2018.

[15] F. Tootoonchian, K. Abbaszadeh, and M. Ardebili, "Novel axial flux brushless resolver analysis and optimization using 3D finite element and DQ model method", *Iranian Journal of Electrical and Electronic Engineering*, Vol. 8, No. 3, pp. 243-258, 2012

[16] R. Alipour-Sarabi, "Use of Resolvers in Limited Rotations," *IEEE Transactions on Energy Conversion*, Vol. 37, No. 3, 2022.

[17] R. Alipour-Sarabi, Z. Nasiri-Gheidari, F. Tootoonchian, and H. Oraee, "Improved Winding Proposal for Wound Rotor Resolver Using Genetic Algorithm and Winding Function Approach," *IEEE Transactions on Industrial Electronics*, Vol. 66, No. 2, pp. 1325-1334, 2019.

[18] M. Alemi-Rostami, R. Alipour-Sarabi, G. Rezazadeh, Z. Nasiri-Gheidari, and H. Oraee, "Design Optimization of a Double-Stage Resolver," *IEEE Transactions on Vehicular Technology*, Vol. 68, No. 6, pp. 5407-5415, 2019.

[19] A. Moheyseni, Z. Nasiri-Gheidari, and R. Alipour-Sarabi, "Slotless Disk Type Resolver: A Solution to Improve the Accuracy of Multi-Speed Wound Rotor Resolvers," *IEEE Transactions on Transportation Electrification*, Vol. 8, No. 1, pp. 1493-1500, 2022.

F. Tootoonchian received the B.Sc. and M.Sc. degrees in electrical engineering from the Iran University of Sciences and Technology, Tehran, Iran, in 2000 and 2007, respectively, and the Ph.D. degree from the K. N. Toosi University of Technology, Tehran, in 2012. He is currently an Assistant Professor with the Department of Electrical Engineering, Iran University of Sciences and Technology. His research interests include design, optimization, finite-element analysis, and prototyping of ultrahigh-speed electrical machines and ultrahigh-precision electromagnetic sensors.

M. Amiri is currently M.Sc. student in School of Advanced Technologies, Iran University od Science and Technology. His research interests include design and optimization of electrical machines, Arduino programming, linear control systems, and machine learning.